Journal of Alloys and Compounds 1003 (2024) 175583

Contents lists available at ScienceDirect

Journal of Alloys and Compounds

journal homepage: www.elsevier.com/locate/jalcom

Effect of thulium on promotion of dose-response behaviour of yttria based rods by Electron Paramagnetic Resonance

S.C. Santos *, O. Rodrigues Jr, L.L. Campos

Instituto de Pesquisas Energeticas e Nucleares – IPEN, Av. Prof. Lineu Prestes 2242, Cidade Universitaria, Sao Paulo, Brazil

ARTICLE INFO

Keywords:
Yttria
Thulium oxide
Rare earths
EPR
Dosimetry
Ceramic processing

ABSTRACT

Radiation dosimetry demands a continuos innovation in materials development. Yttria (Y_2O_3) exhibits intrinsic lattice features that enable doping with other rare-earth ions, resulting in improvement of its solid state characteristics. This work aims to evaluate thulium (Tm) effect on promotion of dose-response behaviour of yttria (YTm) rods by Electron Paramagnetic Resonance (EPR). YTm rods were irradiated with gamma (^{60}Co) doses from 0.001 to 150 kGy and evaluated by EPR, with an X-band EPR, and at room temperature. According to results, YTm rods exhibited a linear dose-response behaviour in a range of dose from 0.001 to 1 kGy. In addition, the fading of EPR signal during 288 h was achieved up to 88 %. These findings indicate that thulium-yttria is a promising material for radiation dosimetry.

1. Introduction

Radiation dosimetry aims to measure the absorbed dose in a given substance which was previously exposed to ionizing radiation [1–5]. Thus, radiation dosimetry is necessary for all applications where ionizing radiation is used as nuclear facilities [6], clinical [7], sterilizing [8], industry [9], and space [10].

Among dosimetry techniques, Electron Paramagnetic Resonance (EPR) is a powerful, non-destructive and non-invasive characterization technique to detect free radicals characteristic in a given substance, and those induced by synthesis and processing procedures, including radiation [11–14]. Some induced radicals present short lifetimes and their identification is hard, whereas some are stable and can be used as probes for radiation doses. Considering an EPR spectra, the peak-to-peak amplitude (PPA) of the major EPR signal is proportional to the number of free radicals (spins) in a sample, and the number of radicals is proportional to the absorbed dose in the sample. Moreover, the PPA is proportional to sample mass and also depends on the measuring parameters as reported elsewhere [15–22].

Radiation dosimetry demands a continuous development of new materials [23–27]with the aim to improve precision and security in practices where ionizing radiation is used. Based on this context, studies on rare-earth based materials for this purpose have been reporting promising results. From the Periodic Table of Elements, rare-earths are from lanthanum (La) to lutetium (Lu) series, including yttrium (Y) and Scandium (Sc). Rare-earths [28] constitute a special class of materials due to their unique chemical and physical properties (photonic [29], electrical [30], electronic [31]) and present a wide range of applicability since agriculture to aerospace industry. Thus, rare-earth materials have been assigned as critical materials [32]. Our research group found out that EPR response of yttria rods was improved by doping with europium (2 at%Eu, atomic percentage) in a range of dose from 0.001 to 10 kGy. Besides, a substantial enhancement of EPR response of thulium-yttria powders was also observed as ranging thulium content from 0 to 1.5 at%Tm [33].

Taking in account the innovative results reported by the group, the present study aims to evaluate thulium (Tm) effect on promotion the dose-response behavior of yttria based rods by EPR. These findings will be useful parameters to advance toward formation of new materials for application in high dose dosimetry, as radiotherapy and industrial procedures.

2. Experimental

Thulium-yttria rods (YTm) with 0.1 at%Tm (atomic percentage, at%) were formed by an eco-friendly bio-prototyping method as reported previously [34]. Thulium concentration of 0.1 at%Tm provides remarkable improvement in Electron Paramagnetic Resonance (EPR) response of yttria, as reported in our previous study[35].

The ceramic rods were characterized by Optical Microscopy (OM,

* Corresponding author.
E-mail address: silas.cardoso@alumni.usp.br (S.C. Santos).

https://doi.org/10.1016/j.jallcom.2024.175583
Received 7 May 2024; Received in revised form 11 June 2024; Accepted 14 July 2024
Available online 15 July 2024

Nikon SMZ1270); Scanning Electron Microscopy (SEM, INCAx-act, Oxford Instruments); and X-ray diffraction (XRD, Rigaku Multiflex, Japan), with an angular range (2θ) from 15 to 70º, scanning of 0.5º.min^{-1} and Kα source. Pycnometric density (ρ_p) was evaluated by using a helium gas pycnometer (Micrometrics 1330), where ρ_s-value is achieved according to Eq. 1[36].

$$\rho_p = \left(\frac{w}{V_p}\right)[g.cm^{-3}] \quad (1)$$

Where, w is the weight of sample, and V_p is the powder volume.

The identification of the crystalline phase from the observed XRD pattern was based on Crystallography Open Database (COD) [37–39]. Besides, Rietveld structure refinement, the mean crystallite size (d_c), theoretical density from observed XRD pattern (ρ_{XRD}), and including electron density distribution of the powdered samples were performed by the open source XRD and Rietveld Refinement software, PROFEX [40]. Furthermore, ball-and-stick and polyhedral representations of the unit cell of a YTm composition were formed by using Vesta [41] software.

Batches containing three ceramic rods each one were irradiated with gamma source (^{60}Co), with range of dose from 0.001 to 150 kGy in electronic equilibrium condition, and at room temperature. Radiation induced defects and radicals were characterized by electron paramagnetic resonance at room temperature and atmosphere using an X-band EPR spectrometer (Bruker EMX PLUS).

EPR spectra of samples were recorded at room temperature and under controlled humidity, using the following parameters: field frequency modulation of 100 kHz, microwave power of 2.5 mW, center field at 320mT, sweep width of 600mT, modulation amplitude of 4 G, time constant of 0.01 ms and, 10 scans, and using DPPH (2, 2-Diphenyl-1-picrylhydrazyl, Bruker) as EPR reference.

The EPR peak-to-peak response of rods was normalized by the average mass of samples and DPPH. The EPR dose response, time and temperature decay curves were plotted considering the average of the peak-to-peak amplitudes (PPA) of samples. The g-factor of EPR spectra were calculated according to Eq.2[42].

$$g = 714.4775\left(\frac{v}{B_0}\right) \quad (2)$$

Where g is the gyromagnetic ratio, B_0 is the magnetic field in gauss (G), and v is the microwave frequency in hertz (GHz).

Despite of SEM images, all experimental data were processed in R programming language [43,44].

3. Results and discussion

The OM and SEM images of a thulium-yttria rod obtained by bio-prototyping, followed by sintering at 1600°C for 2 h under environmental atmosphere are illustrated in Fig. 1. The ceramic rod exhibits uniform shape, with dimensions around of 3.3 ×2.5 mm (height x diameter), and no shaping irregularities as bubbles and asymmetries, as illustrated in Fig. 1a and Fig. 1b, respectively. The surface microstructure (Fig. 1c and Fig. 1d) is constituted by single phase grains bonded at the boundaries due to solid state sintering, forming a triple junction, with no pores. The fracture surface shown in Fig. 1e exhibits cleavage planes of transgranular characteristic, which means that weak interfaces existing in the material provided a pathway for crack propagation across the grains [45,46]. The sintering conditions provided ceramic rods with pycnometric density (ρ_p) of 4.79 g.cm^{-3}±0.009, which corresponds to 95.61 %ρ_{XRD}. While ρ_{XRD} is related with atoms located in the crystal lattice of YTm rods, ρ_p is associated with the real solid volume of YTm rods, where any void space is not considered during measurement. It is clearly evidenced (Fig. 1e) that YTm rods have a microstructure with some porous and void spaces due to particle packing during shaping. Some authors have proposed the use of sintering additives to enhance sintering and the density of ceramics [47–51]. However, it is beyond the aim of this study.

The innovative results on microstructure formation of thulium-yttria reported in this work relies on powder characteristics, such as particle size and shape, particle stabilization, and sintering conditions. It was evidenced that providing the stabilization of particles, which means suspension structure, lead to formation of ceramic components with homogenous microstructure, shape and size, as also reported previously [34]. Comparatively, such achievements have been reported by other authors using sophisticated approaches as, vacuum and hydrogen atmosphere [52–54], Zr^{4+} as grain growth inhibitor [55], high sintering temperature for longer time [56], and flash-sintering [57,58].

YTm rods obtained by bio-prototyping, followed by sintering at 1600 °C for 2 h exhibited a cubic C-type structure (Fig. 2a), composed by sixteen unit formula, C_{3i}, S_6 space group, with three high intensity peaks recorded (angle/plane) at 29.10°/(2,2,2), 48.46°/(4,4,0), and 57.53°/(6,2,2), respectively. As illustrated in Fig. 2b, a small difference between the experimental curve (dark green line) with simulated one (green circles), was observed. Moreover, the peak recorded at 29.10°/(2,2,2) showed the highest signal/noise ratio. Probably the

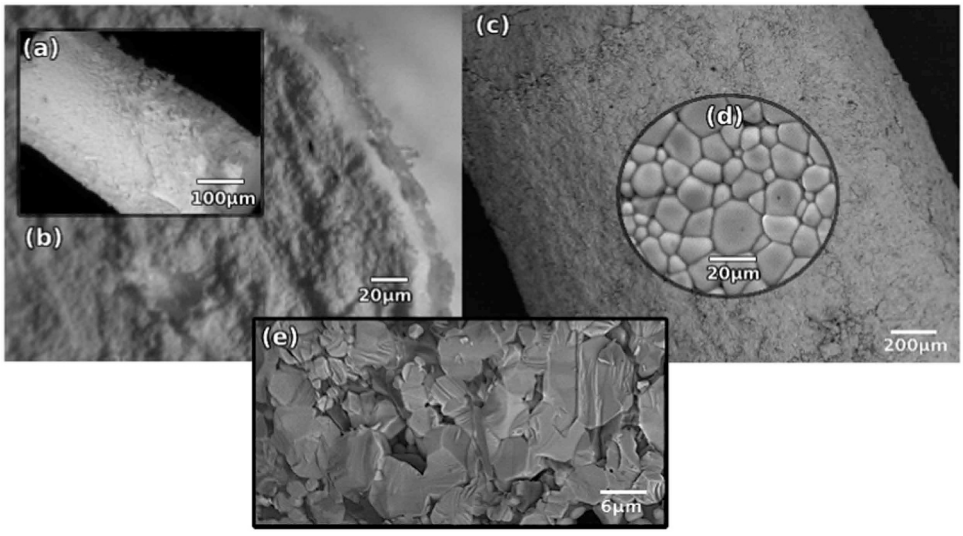

Fig. 1. (a) thulium-yttria rod formed by bio-prototyping and sintering at 1600°C for 2 h under environmental atmosphere; (b) top surface view; (c) side surface view; (d) side surface microstructure, and (e) inner microstructure exhibiting cleavage planes due to transgranular fracture.

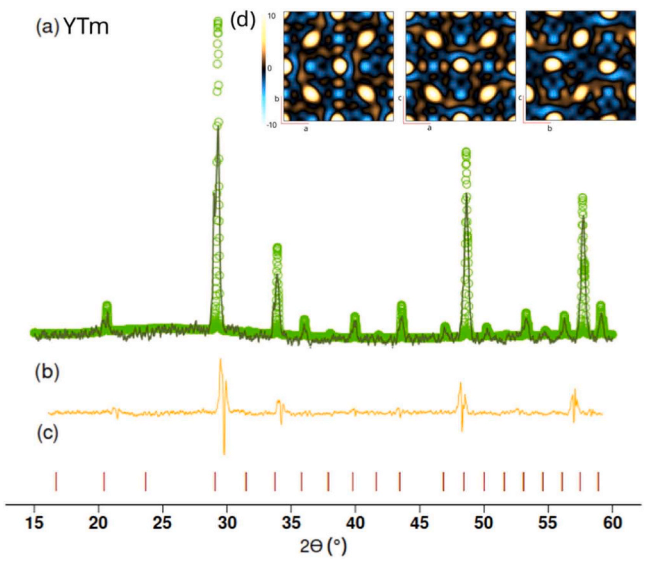

Fig. 2. Rietveld refinement of the XRD pattern observed of YTm rod: (a) dark green line represents the experimental data, while green circles are the simulated pattern; (b) orange line is the difference pattern (experimental – simulated); (c) straight lines are the indexed peaks according to BGMN structure file 04–005–4378; and (d) electron density maps of the unit cell as a function of lattice planes (b-a), (c-a), and (c-b), respectively.

enhancement of peaks size and shape can be performed by increasing sintering time of samples, which in turn, can reduce signal/noise ratio. The following Rietveld fitting results demonstrated that the refinement of the crystal structure was performed accordingly, where the weighted residual square sum (R_{wp}) was 29.02, the possible minimum value for R_{wp} (R_{exp}) was 30.90, quality parameter (χ_2) was 0.88, and crystal density (ρ_{XRD}) was 5.03.gcm^{-3}.

Based on literature [59,60], the cubic C-type form is the most predominant structure for most rare earth sesquioxides (RE_2O_3). Despite of that, yttria can also present A-type (monoclinc), B-type (hexagonal), and C-type (cubic) according to synthesis and processing conditions. All diffraction peaks (Fig. 2c) are in associated with Cubic C-type yttria in accordance with BGMN structure file (04–005–4378), which reveals doping yttria with thulium was effective. According to electron density maps (Fig. 2d), it is seen that yttria lattice is less closed packed, exhibiting large vacancies for Y (bright yellow) and O (dark yellow) planes, as reported by Yong-Nian et al. [61]. These intrinsic vacancies enable the incorporation of RE ions into yttria lattice, forming new yttria based materials with enhanced characteristics/response.

In Fig. 3 is illustrated the EPR spectra of thulium-yttria rods sintered at 1600°C for 2 h in environmental air. Based on results, three EPR peaks assigned as (P_1), (P_2) and (P_3) were recorded at 350mT, 356mT, and 368mT, with the following g-values 2.0126, 1.9787, and 1.9141, respectively. On the other hand, thulium-yttria powders exhibited an EPR spectra with two resonance peaks (P_1 and P_2) recorded at 350mT and 164mT, respectively [33]. This result indicates P_3 peak was promoted by sintering at 1600°C for 2 h under environmental air.

The paramagnetic defect P_1 recorded at 350mT is due to interstitial O^{2-} ion in the lattice, commonly addressed as superoxide ion, which is generated by adsorption of molecular oxygen from atmosphere, as reported elsewhere [62–67]. Moreover, P_2 defect is associated to F^+ centres charged vacancy oxygen, which have one remaining electron. Besides, P_3 defect is ascribed to the presence of the Tm^{3+} ions located at S_6, C_{3i} and C_2 positions of yttria crystal lattice. The achievements reported in the present study reveal that conditions of powder processing, which includes synthesis, have influence on the EPR response of yttria. As yttria exhibits cubic C-type form, its lattice presents intrinsic oxygen vacancies that can produce F centres [68], as well as enable the insertion of other rare-earth ions (Ce^{3+} [69], Yb^{3+}/ Pr^{3+} [70], Nd^{3+} [71], La^{3+} [72]) to form new materials.

As exposed to ionizing radiation up to 150 kGy using ^{60}Co (Fig. 3) and (Fig. 4), it was noticed that peak-to-peak amplitude of P_1 peak increases as a function of dose from 0 (no dose) to 1 kGy, while apart from 1 kGy dose-response relation is not maintained. In fact, doses above

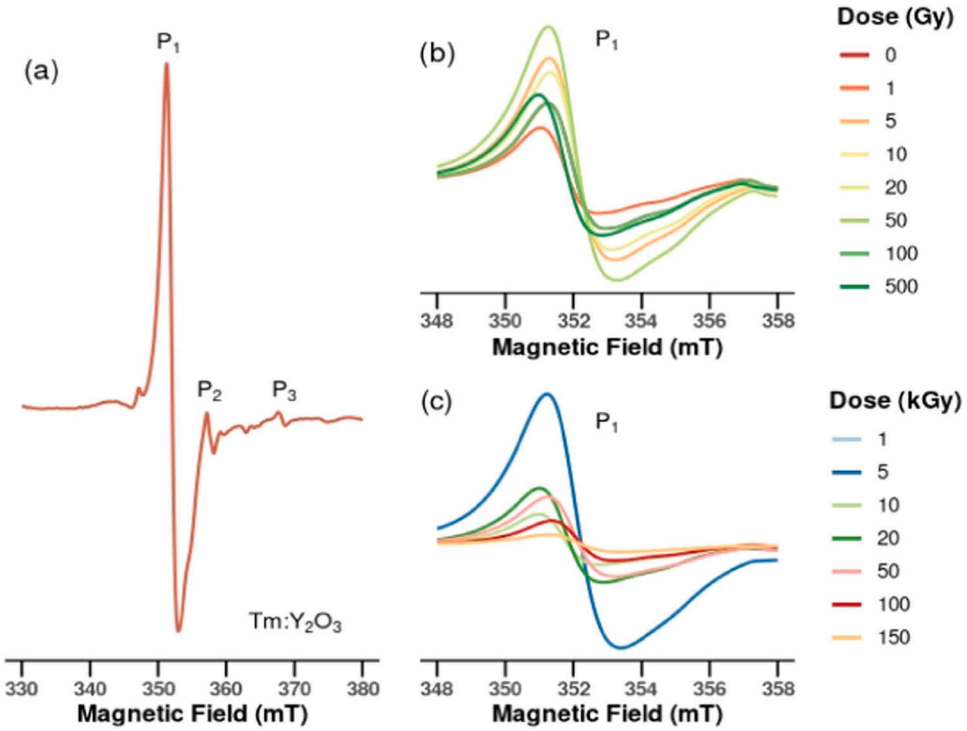

Fig. 3. EPR spectra of YTm rods sintered at 1600°C for 2 h in air atmosphere, and recorded in a range of magnetic field (a) from 330 to 380mT (general view); evolution of P_1 peak as a function of dose from (b) from 0 to 500 Gy, and (c) from 1 to 150 kGy.

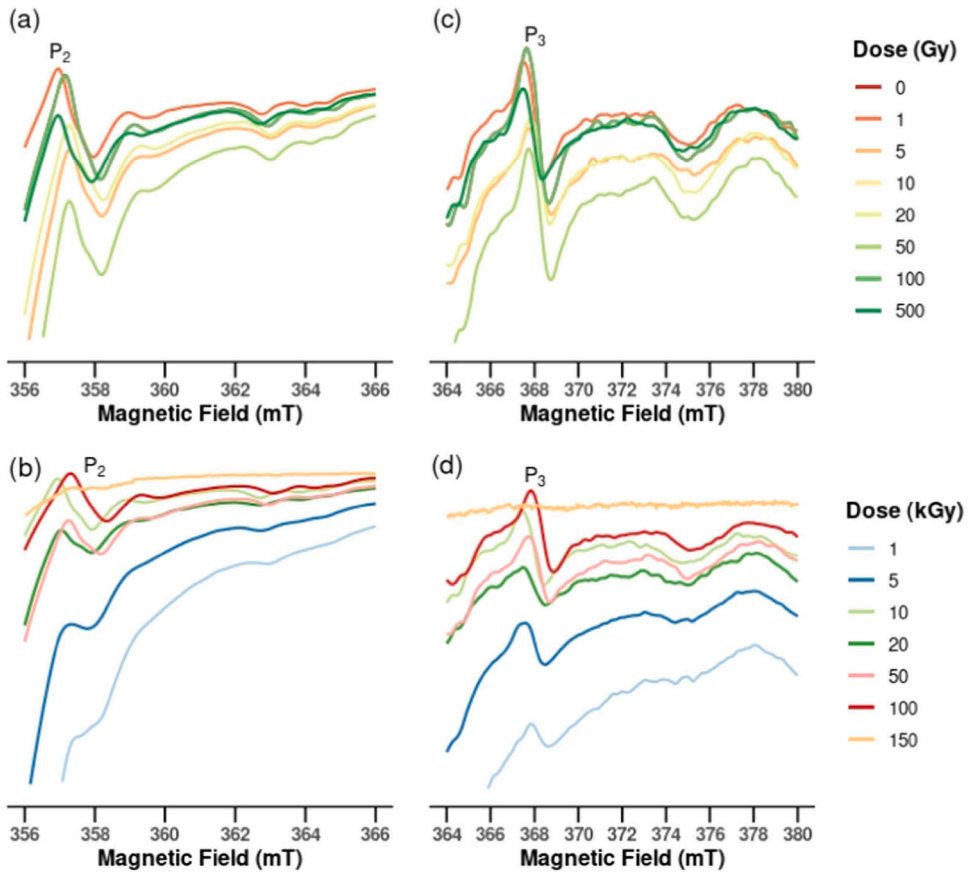

Fig. 4. EPR spectra of YTm rods sintered at 1600°C for 2 h in air atmosphere, recorded in a range of magnetic field from 356 to 380mT, where the evolution of (a) P_2 and (c) P_3 peak as a function of dose from 0 to 500 Gy, and from 1 to 150 kGy (b) P_2, and (d) P_3 are illustrated.

1 kGy tend reduce radicals formation, by recombination effects and releasing of those electrons from forbidden band to valence band. Considering previous studies performed by the group on rare-earth based materials, it was observed that "pure" yttria rods [73] exhibited two EPR peaks (p_1) and (p_2) recorded at 352mT and 357mT, respectively. In addition, the EPR peak named as p_1 is associated with oxygen vacancies. Moreover, doping yttria with europium led to formation of ceramic rods with two EPR peaks recorded at 163mT and 248mT. These achievements reveal doping using rare-earth ions provides significant changes on yttria paramagnetic response.

The signal amplitude of P_1 peak as a function of dose for yttria based rods exposed to doses up to 150 kGy was evaluated and the results are illustrated in Fig. 5. According to results, it is clearly evidenced a regular dose response behaviour for ceramic rods exposed to doses up to 1 kGy (red dot line). On the other hand, doses above 1 kGy led to decrease of EPR signal of rods, which means ionizing radiation induces new radicals which combine with others and then reduces EPR signal. Comparatively to our previous studies, while "pure" yttria exhibited a very low dose-response behaviour in a range of dose from 0.001 to 150 kGy, while doping it with 2 at%Eu (atomic percentage) enhanced dose-response behaviour of rods in a range of dose from 0.001 to 10 kGy [74]. Even though doping with Tm enhanced the dose-response behavior in a shorter range of those (0.001 – 1 kGy), the improvement was very significant and promising for radiation dosimetry in this range of dose.

The fading of the EPR signal of YTm rods corresponding to P_1 peak is illustrated in Fig. 6. Based on results, rods irradiated with 10 kGy and 100 kGy exhibited a significant decrease of the EPR relative signal from 100 % to 93 % and 87 % during 48 h, respectively. While, those irradiated with 100 Gy and 1 kGy exhibited 96 % and 98 %, respectively. During 288 h the fading of ceramic rods exposed to 0.1 up to 100 kGy was recorded as follows: 88 %, 82 %, 74 %, and 70 %, respectively.

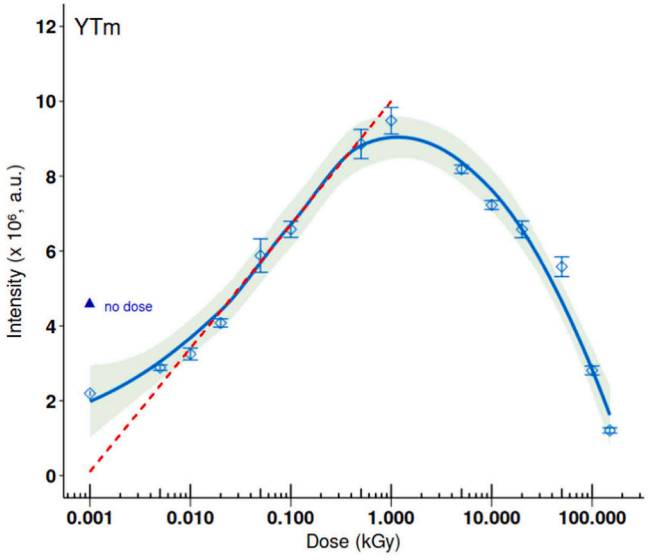

Fig. 5. Peak to peak amplitude of EPR signal (P_1) of YTm rods as a function of dose from 0.001 to 150 kGy.

Considering the results of dose-response illustrated in Fig. 5, ceramic rods exposed to doses which are in the linear region (0.001–1 kGy) presents more stability of signal during time.

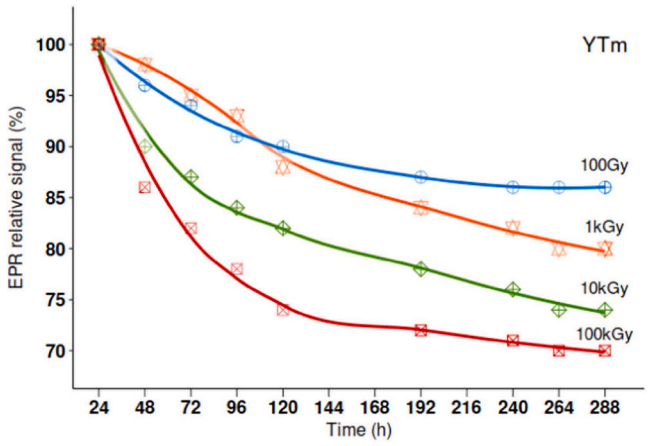

Fig. 6. Fading of the EPR signal (P_1) of YTm rods irradiated with up to 100 kGy and recorded during 288 h.

4. Conclusion

Thulium-yttria (YTm) rods, with pycnometric density of 95.61 %, and cubic C-type structure, were successfully obtained by bio-prototyping, followed by sintering at 1600°C for 2 h under environmental air. Doping yttria with 0.1 at% of thulium (at%, atomic percentage) provided considerable improvement on EPR response of the ceramic rods as exposed to doses up to 150 kGy (^{60}Co). The EPR dose response behaviour of YTm rods exhibited a linear character from 0.001 up to 1 kGy. Above 1 kGy the EPR signal started decreasing consistently, which suggests a recombination of electronic defects. The fading during 288 h of ceramic rods exposed to 0.1 up to 100 kGy was recorded as follows: 88 %, 82 %, 74 %, and 70 %, respectively. The present results constitute important parameters to advance toward new materials for radiation dosimetry.

CRediT authorship contribution statement

S.C. Santos: Conceptualization, Formal analysis, Methodology, Writing – original draft, Writing – review & editing. **O. Rodrigues Jr:** Data curation, Software, Validation. **L.L. Campos:** Funding acquisition, Project administration, Supervision, Visualization.

Declaration of Competing Interest

The authors declare that they have no known competing financial interests or personal relationships that could have appeared to influence the work reported in this paper

Data Availability

The authors do not have permission to share data.

Acknowledgements

São Paulo Research Foundation (FAPESP), grant#2022/06695-0; National Council for Scientific and Technological Development (CNPq); and Coordination for Improvement of High Degree People (CAPES).

References

[1] C. Lawhn-Heath, T.A. Hope, J. Martinez, E.K. Fung, J. Shin, Y. Seo, R.R. Flavell, Dosimetry in radionuclide therapy: the clinical role of measuring radiation dose, Lancet Oncol. 23 (2022) e75–e87, https://doi.org/10.1016/S1470-2045(21)00657-4.

[2] S.A. Graves, R.F. Hobbs, Dosimetry for optimized, personalized radiopharmaceutical therapy, Semin. Radiat. Oncol. 31 (2021) 37–44, https://doi.org/10.1016/j.semradonc.2020.07.008.

[3] G.M. Currie, E.M. Rohren, Radiation dosimetry, artificial intelligence and digital twins: old dog, new tricks, Semin. Nucl. Med. 53 (2023) 457–466, https://doi.org/10.1053/j.semnuclmed.2022.10.007.

[4] J.W. Poston, Dosimetry, in: R.A. Meyers (Ed.), Encyclopedia of Physical Science and Technology (Third Edition), Academic Press, New York, 2003, pp. 603–650, https://doi.org/10.1016/B0-12-227410-5/00185-X.

[5] C. Lawhn-Heath, T.A. Hope, J. Martinez, E.K. Fung, J. Shin, Y. Seo, R.R. Flavell, Dosimetry in radionuclide therapy: the clinical role of measuring radiation dose, Lancet Oncol. 23 (2022) e75–e87, https://doi.org/10.1016/S1470-2045(21)00657-4.

[6] Ž. Knežević, M. Majer, Z. Baranowska, O.C. Bjelac, G. Iurlaro, N. Kržanović, F. Mariotti, M. Nodilo, S. Neumaier, K. Wołoszczuk, M. Živanović, Investigations into the basic properties of different passive dosimetry systems used in environmental radiation monitoring in the aftermath of a nuclear or radiological event, Radiat. Meas. 146 (2021) 106615, https://doi.org/10.1016/j.radmeas.2021.106615.

[7] C. Fiorino, R. Jeraj, C.H. Clark, C. Garibaldi, D. Georg, L. Muren, W. van Elmpt, T. Bortfeld, N. Jornet, Grand challenges for medical physics in radiation oncology, Radiother. Oncol. 153 (2020) 7–14, https://doi.org/10.1016/j.radonc.2020.10.001.

[8] V. Kalia, D. Joseph, in: E.B.T.-E. of N.E. Greenspan (Ed.), Medicine: Sterilization, Elsevier, Oxford, 2021, pp. 224–235, https://doi.org/10.1016/B978-0-12-819725-7.00005-2.

[9] A. Oresegun, A. Basaif, Z.H. Tarif, H.A. Abdul-Rashid, S.A. Hashim, D.A. Bradley, Radioluminescence of silica optical fibre scintillators for real-time industrial radiation dosimetry, Radiat. Phys. Chem. 188 (2021) 109684, https://doi.org/10.1016/j.radphyschem.2021.109684.

[10] W. Tinganelli, F. Luoni, M. Durante, What can space radiation protection learn from radiation oncology? Life Sci. Space Res. 30 (2021) 82–95, https://doi.org/10.1016/j.lssr.2021.06.002.

[11] N. Hajiloo, F. Ziaie, A comparison study of dosimetry response of nano-crystalline hydroxyapatite via the EPR technique: effect of fabrication process, Results Phys. 47 (2023) 106338, https://doi.org/10.1016/j.rinp.2023.106338.

[12] S. Azam, V. Kurashov, J.H. Golbeck, S. Bhattacharyya, S. Zheng, S. Liu, Comparative 6+studies of environmentally persistent free radicals on nano-sized coal dusts, Sci. Total Environ. 878 (2023) 163163, https://doi.org/10.1016/j.scitotenv.2023.163163.

[13] A. Antuzevics, J. Cirulis, G. Krieke, D. Griesiute, A. Beganskiene, A. Kareiva, A. Dubauskas, V. Klimavicius, A. Zarkov, Paramagnetic radiation-induced radicals in calcium pyrophosphate polymorphs, Mater. Chem. Phys. 310 (2023) 128479, https://doi.org/10.1016/j.matchemphys.2023.128479.

[14] A.B. Rech, A. Kinoshita, P.M. Donate, O. Baffa, ESR dosimetry with lithium, potassium, and sodium compounds, Appl. Radiat. Isot. 181 (2022) 110105, https://doi.org/10.1016/j.apradiso.2022.110105.

[15] G.R. Eaton, S.S. Eaton, 2.03 - Electron Paramagnetic Resonance Spectroscopy, in: E.C. Constable, G. Parkin, L.B.T.-C.C.C.I.I.I. Que Jr (Eds.), Elsevier, Oxford, 2021: pp. 44–59. https://doi.org/10.1016/B978-0-12-409547-2.14621-9.

[16] J. Reichenwallner, B. Liu, A.R. Balo, W.-L. Ou, O.P. Ernst, Electron paramagnetic resonance spectroscopy on G-protein-coupled receptors: Adopting strategies from related model systems, Curr. Opin. Struct. Biol. 69 (2021) 177–186, https://doi.org/10.1016/j.sbi.2021.06.003.

[17] I. Stefaniuk, Electron paramagnetic resonance study of impurities and point defects in oxide crystals, Opto-Electron. Rev. 26 (2018) 81–91, https://doi.org/10.1016/j.opelre.2018.02.002.

[18] P.M. Clawin, N.F. Richter, W. Riedel, H. Ronneburg, T. Risse, Electron paramagnetic resonance spectroscopy at surfaces, in: K.B.T.-E. of I.C. Wandelt (Ed.), Elsevier, Oxford, 2018: pp. 129–142. https://doi.org/10.1016/B978-0-12-409547-2.12820-3.

[19] M.J. Davies, Detection and characterisation of radicals using electron paramagnetic resonance (EPR) spin trapping and related methods, Methods 109 (2016) 21–30, https://doi.org/10.1016/j.ymeth.2016.05.013.

[20] E. Bordignon, S. Bleicken, New limits of sensitivity of site-directed spin labeling electron paramagnetic resonance for membrane proteins, Biochim. Et. Biophys. Acta (BBA) - Biomembr. 1860 (2018) 841–853, https://doi.org/10.1016/j.bbamem.2017.12.009.

[21] R. Ahmad, P. Kuppusamy, Theory, instrumentation, and applications of electron paramagnetic resonance oximetry, Chem. Rev. 110 (2010) 3212–3236, https://doi.org/10.1021/cr900396q.

[22] J.P. Klare, Electron paramagnetic resonance of membrane proteins, in: J.C. Lindon, G.E. Tranter, D.W.B.T.-E. of S. and S. (Third E. Koppenaal (Eds.), Academic Press, Oxford, 2017: pp. 442–446. https://doi.org/10.1016/B978-0-12-409547-2.12118-3.

[23] M.A.H. Rushdi, A.A. Abdel-Fattah, M.M. Sherif, Y.S. Soliman, A. Mansour, Strontium sulfate as an EPR dosimeter for radiation technology application, Radiat. Phys. Chem. 106 (2015) 130–135, https://doi.org/10.1016/j.radphyschem.2014.07.009.

[24] M.O. Bal, H. Tuner, Investigation of radiation sensitivity of some tartrate compounds, Radiat. Prot. Dosim. 159 (2014) 199–202, https://doi.org/10.1093/rpd/ncu119.

[25] N.M. Nor, S. Hashim, A.T. Ramli, E. Saion, T. Kadni, EPR dosimeter material properties of potassium tartrate hemihydrate, Radiat. Meas. 87 (2016) 8–12, https://doi.org/10.1016/j.radmeas.2016.02.008.

[26] M. Marrale, M. Brai, A. Barbon, M. Brustolon, Analysis of the spatial distribution of free radicals in ammonium tartrate by pulse EPR techniques, Radiat. Res. 171 (2009) 349–359, https://doi.org/10.1667/RR1358.1.

[27] L.H. Jiang, Y.L. Zhang, X.M. Gong, R. Pang, S. Zhang, C.Y. Li, Q. Su, LiSr4(BO3)3: Ce3+ phosphor as a new material for ESR dosimetry, Appl. Radiat. Isot. 84 (2014) 66–69, https://doi.org/10.1016/j.apradiso.2013.11.029.

[28] S. Santos, O. Rodrigues, L. Campos, A Glance on Rare Earth Oxides: Importance, Reserves, Demand, Applications, Critical Uncertainties, Global Economy, and Zeta Potential Characterization, (2020) 1–22. https://doi.org/10.2174/2405465805999200628095450.

[29] L. Andronic, D. Moldarev, D. Deribew, E. Moons, S.Z. Karazhanov, Photocatalytic self-cleaning properties of thin films of photochromic yttrium oxyhydride, J. Solid State Chem. 316 (2022) 123599, https://doi.org/10.1016/j.jssc.2022.123599.

[30] M. François, V. Lescure, O. Heintz, L. Combemale, F. Demoisson, G. Caboche, Synthesis of Y-doped BaZrO3 proton conducting electrolyte material by a continuous hydrothermal process in supercritical conditions: Investigation of the formation mechanism and electrochemical performance, Ceram. Int. 49 (2023) 25344–25352, https://doi.org/10.1016/j.ceramint.2023.05.070.

[31] D.L. Druffel, M.G. Lanetti, J.D. Sundberg, J.T. Pawlik, M.S. Stark, C.L. Donley, L. M. McRae, K.M. Scott, S.C. Warren, Synthesis and electronic structure of a 3D crystalline stack of mxene-like sheets, Chem. Mater. 31 (2019) 9788–9796, https://doi.org/10.1021/acs.chemmater.9b03722.

[32] C. Bobba, S., Carrara, S., Huisman, J., Mathieux, F., Pavel, European Commission, Critical materials for strategic technologies and sectors in the EU - a foresight study, European Commission Joint Research Centre), 2020. https://doi.org/10.2873/58081.

[33] S.C. Santos, O. Rodrigues, L.L. Campos, Towards a new promising dosimetric material from formation of thulium-yttria nanoparticles with EPR response, Mater. Chem. Phys. 259 (2021) 124005, https://doi.org/10.1016/j.matchemphys.2020.124005.

[34] S.C. Santos, O. Rodrigues, L.L. Campos, Colloidal processing of thulium-yttria microceramics, J. Phys. Chem. Solids 161 (2022) 110420, https://doi.org/10.1016/j.jpcs.2021.110420.

[35] S.C. Santos, Ot. a new promising dosimetric material from formation of thulium-yttria nanoparticles with E. response Rodrigues, L.L. Campos, Towards a new promising dosimetric material from formation of thulium-yttria nanoparticles with EPR response, Mater. Chem. Phys. 259 (2021) 124005, https://doi.org/10.1016/j.matchemphys.2020.124005.

[36] P. (Paul A.) Webb, Clyde. Orr, Analytical methods in fine particle technology, Micromeritics Instrument Corporation, Norcross, Ga, 1997.

[37] A. Vaitkus, A. Merkys, T. Sander, M. Quirós, P.A. Thiessen, E.E. Bolton, S. Gražulis, A workflow for deriving chemical entities from crystallographic data and its application to the crystallography open database, J. Chemin.-. 15 (2023), https://doi.org/10.1186/s13321-023-00780-2.

[38] A. Merkys, A. Vaitkus, A. Grybauskas, A. Konovalovas, M. Quirós, S. Gražulis, Graph isomorphism-based algorithm for cross-checking chemical and crystallographic descriptions, J. Chemin.-. 15 (2023) 25, https://doi.org/10.1186/s13321-023-00692-1.

[39] A. Vaitkus, A. Merkys, S. Gražulis, Validation of the crystallography open database using the crystallographic information framework, J. Appl. Crystallogr. 54 (2021) 661–672, https://doi.org/10.1107/S1600576720016532.

[40] N. Doebelin, R. Kleeberg, Profex: a graphical user interface for the Rietveld refinement program, J. Appl. Crystallogr. 48 (2015) 1573–1580, https://doi.org/10.1107/S1600576715014685.

[41] K. Momma, F. Izumi, VESTA: a three-dimensional visualization of crystal, volumetric and morphology data, J. Appl. Crystallogr. 44 (2011) 1272–1276, https://doi.org/10.1107/S0021889811038970.

[42] J.A. Weil, J.R. Bolton, J.E. Wertz, Electron Paramagnetic Reso- nance, Elementary Theory and Practical Applications, New York, 1994.

[43] R. Core Team, An Introduction to R, 2024. https://cran.r-project.org/ (accessed May 7, 2024).

[44] Hadley Wickham, Danielle Navarro, Thomas Lin Pedersen, ggplot2: Elegant Graphics for Data Analysis, 3rd ed., n.d. https://ggplot2-book.org/.

[45] A.P.B.T.-I. to A.M. Mouritz, ed., 18 - Fracture processes of aerospace materials, in: Woodhead Publishing, 2012: pp. 428–453. https://doi.org/10.1533/9780857095152.428.

[46] M. Anglada, 3 - Assessment of mechanical properties of ceramic materials, in: P. Palmero, F. Cambier, E.B.T.-A. in C.B. De Barra (Eds.), Woodhead Publishing, 2017: pp. 83–109. https://doi.org/10.1016/B978-0-08-100881-2.00003-8.

[47] A. Saintonge, J. Braun, J. Danet, A. Allemand, T. Piquero, S. Beaudet-Savignat, Y. Lepetitcorps, Lowering hexacelsian sintering temperature with additives: solid or liquid phase mechanisms, J. Eur. Ceram. Soc. 44 (2024) 5938–5956, https://doi.org/10.1016/j.jeurceramsoc.2024.03.026.

[48] M. De Lisi, F. Careri, U.M. Attia, K. Essa, Effect of different additives and sintering regimes on the optical properties of DLP printed translucent alumina, Ceram. Int. 50 (2024) 26065–26076, https://doi.org/10.1016/j.ceramint.2024.04.348.

[49] S. Jamale, B. Venkata Manoj Kumar, B4C-SiC composites with tuneable mechanical properties: role of Al2O3 - Y2O3 sintering additives, J. Alloy. Compd. 976 (2024) 172954, https://doi.org/10.1016/j.jallcom.2023.172954.

[50] S.A. Belyakov, A.S. Lesnichyova, V.B. Balakireva, A.P. Tarutin, L.A. Dunyushkina, ZnO sintering additive without negative impact on proton-conducting SrHf0.8Sc0.2O3-δ electrolyte, Ceram. Int. (2024), https://doi.org/10.1016/j.ceramint.2024.04.331.

[51] Y. Shan, C. Wei, L. Ma, H. Guo, X. Han, J. Li, J. Xu, Fast densification mechanism of highly transparent AlON ceramics pressureless sintered by co-doping Y2O3 and MgO additives, J. Eur. Ceram. Soc. 44 (2024) 2395–2407, https://doi.org/10.1016/j.jeurceramsoc.2023.11.039.

[52] R.A. Lefever, J. Matsko, Transparent yttrium oxide ceramics, Mater. Res. Bull. 2 (1967) 865–869, https://doi.org/10.1016/0025-5408(67)90096-7.

[53] Y. Huang, D. Jiang, J. Zhang, Q. Lin, Fabrication of transparent lanthanum-doped yttria ceramics by combination of two-step sintering and vacuum sintering, J. Am. Ceram. Soc. 92 (2009) 2883–2887, https://doi.org/10.1111/j.1551-2916.2009.03312.x.

[54] T. Ikegami, J.-G. Li, T. Mori, Y. Moriyoshi, Fabrication of transparent yttria ceramics by the low-temperature synthesis of yttrium hydroxide, J. Am. Ceram. Soc. 85 (2002) 1725–1729, https://doi.org/10.1111/j.1151-2916.2002.tb00342.x.

[55] P..-L. Grain Boundary Mobility in Y2O3: Defect Mechanism and Dopant EffectsChen, I.-W. Chen, Grain Boundary Mobility in Y2O3: Defect Mechanism and Dopant Effects, Journal of the American Ceramic Society 79 (1996) 1801–1809. https://doi.org/doi:10.1111/j.1151-2916.1996.tb07998.x.

[56] D.J. Sordelet, M. Akinc, Sintering of monosized, spherical yttria powders, J. Am. Ceram. Soc. 71 (1988) 1148–1153, https://doi.org/10.1111/j.1151-2916.1988.tb05807.x.

[57] H. Yoshida, Y. Sakka, T. Yamamoto, J.-M. Lebrun, R. Raj, Densification behaviour and microstructural development in undoped yttria prepared by flash-sintering, J. Eur. Ceram. Soc. 34 (2014) 991–1000, https://doi.org/10.1016/j.jeurceramsoc.2013.10.031.

[58] R. Raj, Joule heating during flash-sintering, J. Eur. Ceram. Soc. 32 (2012) 2293–2301, https://doi.org/10.1016/j.jeurceramsoc.2012.02.030.

[59] K. Riener, N. Albrecht, S. Ziegelmeier, R. Ramakrishnan, L. Haferkamp, A. B. Spierings, G.J. Leichtfried, Influence of particle size distribution and morphology on the properties of the powder feedstock as well as of AlSi10Mg parts produced by laser powder bed fusion (LPBF), Addit. Manuf. 34 (2020) 101286, https://doi.org/10.1016/j.addma.2020.101286.

[60] J.P. Coutures, R. Verges, M. Foex, Comparison of solidification temperatures of different rare earth sesquioxides; effect of atmosphere, Rev. Int. Des. Hautes Temp. Et. Des. Refract. 12 (1975) 181–185.

[61] Y.N. Xu, Z.Q. Gu, W.Y. Ching, Electronic, structural, and optical properties of crystalline yttria, Phys. Rev. B 56 (1997) 14993–15000, https://link.aps.org/doi/10.1103/PhysRevB.56.14993.

[62] J.H. Lunsford, Esr of adsorbed oxygen species, Catal. Rev. -Sci. Eng. 8 (1973) 135–157.

[63] A. Fujimori, Spectroscopic evidence for localized and extended F-symmetry states in Ceo2 - comment, Phys. Rev. Lett. 53 (1984) 2518, https://doi.org/DOI 10.1103/PhysRevLett.53.2518.

[64] E. Wuilloud, B. Delley, W.D. Schneider, Y. Baer, Spectroscopic evidence for localized and extended F-symmetry states in Ceo2 - reply, Phys. Rev. Lett. 53 (1984) 2519, https://doi.org/DOI 10.1103/PhysRevLett.53.2519.

[65] A. Pfau, K.D. Schierbaum, The electronic structure of stoichiometric and reduced CeO2 surfaces: an XPS, UPS and HREELS study, Surf. Sci. 321 (1994) 71–80, https://doi.org/10.1016/0039-6028(94)90027-2.

[66] H. Norenberg, G.A.D. Briggs, Defect structure of nonstoichiometric CeO2(111) surfaces studied by scanning tunneling microscopy, Phys. Rev. Lett. 79 (1997) 4222–4225, https://doi.org/DOI 10.1103/PhysRevLett.79.4222.

[67] D.R. Mullins, S.H. Overbury, D.R. Huntley, Electron spectroscopy of single crystal and polycrystalline cerium oxide surfaces, Surf. Sci. 409 (1998) 307–319, https://doi.org/Doi 10.1016/S0039-6028(98)00257-X.

[68] T. Herzig, T. Lühmann, P. Räcke, C. Scheuner, S. Pezzagna, J. Meijer, Chapter One - Color center formation by deterministic single ion implantation, in: C.E. Nebel, I. Aharonovich, N. Mizuochi, M. Hatano (Eds.), Semiconductors and Semimetals, Elsevier, 2021, pp. 1–30, https://doi.org/10.1016/bs.semsem.2020.09.001.

[69] Q. Wang, Q. Liu, P. Chen, Z. Dai, X. Li, L. Zhang, T. Xie, J. Li, Highly transparent Ce-doped yttria stabilized zirconia ceramics with bright red color, Opt. Mater. 129 (2022) 112484, https://doi.org/10.1016/j.optmat.2022.112484.

[70] L.R.R. Nunes, H.P. Labaki, F.J. Caixeta, R.R. Gonçalves, Yb3+ influence on NIR emission from Pr3+-doped spherical yttria nanoparticles for advances in NIR I and NIR II biological windows, J. Lumin. 241 (2022) 118485, https://doi.org/10.1016/j.jlumin.2021.118485.

[71] L. Gan, Y.-J. Park, L.-L. Zhu, H.-N. Kim, J.-W. Ko, J.-W. Lee, Highly transparent Nd-doped yttria ceramics fabricated by hot pressing with ZrO2 and La2O3 as sintering additives, J. Alloy. Compd. 763 (2018) 192–198, https://doi.org/10.1016/j.jallcom.2018.05.304.

[72] L. Gan, Y.-J. Park, L.-L. Zhu, S.-I. Go, H. Kim, J.-M. Kim, J.-W. Ko, Fabrication and properties of La2O3-doped transparent yttria ceramics by hot-pressing sintering, J. Alloy. Compd. 695 (2017) 2142–2148, https://doi.org/10.1016/j.jallcom.2016.11.059.

[73] S.C. Santos, O. Rodrigues, L.L. Campos, EPR dosimetry of yttria micro rods, J. Alloy. Compd. (2018), https://doi.org/10.1016/j.jallcom.2018.01.315.

[74] S.C. Santos, O. Rodrigues, L.L. Campos, EPR response of yttria micro rods activated by europium, J. Alloy. Compd. (2018), https://doi.org/10.1016/j.jallcom.2018.06.063.